Available online at www.sciencedirect.com

SciVerse ScienceDirect

Ceramics International 39 (2013) 8521–8526

CERAMICS INTERNATIONAL

www.elsevier.com/locate/ceramint

Short communication

Biotemplated multichannel mesoporous bioactive glass microtubes as a drug carrier

Wentao Liu[a], Xin Wang[a], Xiaohan Gao[a], Xiaofeng Chen[a], Xinghua Yu[a], Hongsu Wang[a,b,*], Xuming Deng[a,**]

[a]*Key Laboratory of Zoonosis, Ministry of Education, Institute of Zoonosis, College of Veterinary Medicine, Jilin University, Changchun 130062, PR China*

[b]*Teaching Center of Basic Courses, Jilin University, Changchun 130062, PR China*

Received 12 November 2012; received in revised form 28 February 2013; accepted 12 March 2013
Available online 21 March 2013

Abstract

Multichannel mesoporous bioactive glass (MBG) microtubes were synthesized using Pluronic P123 and wool sponges as templates. The fine one-dimensional multichannel structures of the biological templates were faithfully duplicated. The wool sponges not only created pores but also helped increase the growth rate of hydroxycarbonate apatite in simulated body fluid (SBF). The biocompatibilities were also evaluated by culturing the MC3T3-E1 cells on the mesoporous bioactive glass microtubes. The MBG microtubes exhibited delicate multichannel tubular structures, bioactivities, biocompatibilities and the capability for sustained drug delivery. The data provided evidence that the material had excellent potential for applications in the fields of tissue engineering and drug storage.

Keywords: A. Sol–gel processes; B. Porosity; D. Glass ceramics; E. Biomedical applications

1. Introduction

Materials with hollow micro-/nanotubular structures have attracted growing research interest for many applications such as catalysis support, drug/gene delivery and medical diagnostics [1–5]. Tubular carriers are emerging as one of the most promising delivery vehicles due to their significant advantages over spherical micro-/nanoparticles, including remarkably high drug-carrying capacities and prolonged circulation time [6–10]. While much of the literature thus far has focused on the synthesis and basic properties of one-dimensional (1D) structures, demonstrations of more advanced applications and controlled assemblies are emerging [11,12]. Moreover, delicate multichannel (or multichamber) tubular structures have been adapted in a number of animals during the course of evolution, including the feathers of many bird species. The unique internal configurations of the multichannel tubular structures found in nature have many attractive features of interest to scientists [13,14].

Recently, mesoporous bioactive glass (MBG) has been widely studied because of its potential in bone or tooth reconstruction and substitution [15–18]. However, the mesoscale pores of the MBG are too small to promote cell adhesion and nutrition transportation [19]. Therefore, merging the mesoporous structures of the MBG and the tubular macroporous morphologies would give rise to a new class of multifunctional materials. In this process, tubular structures are achieved through sol–gel method-based template synthesis. Because the structures of the products are severely limited by the simple morphology of their artificial template substrates, a biotemplate strategy could provide a short cut for producing functional materials with complex natural structures [20–22]. Biotemplates with sophisticated micro-/nanostructures are difficult to obtain, even with the most technologically advanced synthetic methodologies. For this purpose, our group first successfully prepared hierarchically macro-/mesoporous

*Corresponding author at: Key Laboratory of Zoonosis, Ministry of Education, Institute of Zoonosis, College of Veterinary Medicine, Jilin University, Changchun 130062, PR China. Tel.: +86 431 87836471; fax: +86 431 87836161.

**Corresponding author.

E-mail addresses: wanghs@jlu.edu.cn (H. Wang), dengxm@jlu.edu.cn (X. Deng).

0272-8842/$ - see front matter © 2013 Elsevier Ltd and Techna Group S.r.l. All rights reserved.
http://dx.doi.org/10.1016/j.ceramint.2013.03.034

MBG ceramic scaffolds using natural Mediterranean Sea sponges as the biotemplate [23]. The synthesized materials exhibited some ability for apatite mineralization and drug delivery in bone regeneration. Therefore, the synthesis of one-dimensional inorganic hollow MBG microtubes was of interest for enhancing the performance of the previously mentioned scaffold.

In the present work, MBG microtubes with improved structural features and complicated hierarchical morphologies were successfully produced using the sol–gel method accompanied by biotemplate synthesis. The result was that MBG microtubes exhibited accelerated bioactivity, forming a bonelike apatite phase on the surface, and were highly biocompatible and capable of sustained drug delivery. The dexamethasone (DEX) adsorption capacity of the synthesized MBG microtubes was 2 times higher, with a more uniform rate of release and a longer release time than that of the MBG scaffolds using the natural Mediterranean Sea sponge as a biotemplate [23].

2. Experiments

2.1. Synthesis of MBG microtubes

First, highly ordered mesoporous bioactive glasses (MBG) (molar ratio: Si/Ca/P = 80/15/5) were synthesized using the nonionic block copolymer pluronic P123 ($EO_{20}PO_{70}EO_{20}$) as a surfactant [15]. Triethyl phosphate (TEP), tetraethyl orthosilicate (TEOS) and $Ca(NO_3)_2 \cdot 4H_2O$ were used as SiO_2, P_2O_5, and CaO sources, respectively. In a typical synthesis, 4 g P123 was dissolved in 60 mL ethanol with 1.0 g of a 0.5 M HCl solution. Then, 6.7 g TEOS, 0.73 g TEP, and 1.4 g $Ca(NO_3)_2 \cdot 4H_2O$ were added. The solution was stirred at room temperature for 24 h. The P123 served as soft templates for the subsequent formation of mesopores. Second, the solution was introduced into a hard template consisting of wool sponges. The excess solution was removed and the remainder allowed to evaporate at room temperature for 24 h. This procedure was repeated 6 times. Third, the organic-phase soft template was removed via calcination at 600 °C for 8 h. The MBG microtubes were then obtained.

2.2. In vitro mineralization

The ionic composition of the as-prepared simulated body fluid (SBF) solution was similar to that of human body plasma with a molar composition of 142.0, 5.0, 2.5, 1.5, 147.8, 4.2, 1.0 and 0.5 for Na^+, K^+, Ca^{2+}, Mg^{2+}, Cl^-, HCO_3^-, HPO_4^{2-} and SO_4^{2-}, respectively (pH = 7.4) [24]. The 1 g MBG tubular scaffolds were soaked in 50 mL SBF with shaking at 37 °C for 6, 24, 72 and 168 h.

2.3. Drug loading and release from the MBG microtubes

A 0.2 g sample of the MBG microtubes was added to 200 mL of a 1 mg mL^{-1} DEX/ethanol solution and soaked for 24 h at room temperature. The MBG/DEX microtubes were obtained after drying at 50 °C for 24 h. Filtrate (1.0 mL) was sucked and properly diluted to determine the drug-loading amount by High Performance Liquid Chromatography (HPLC). The DEX release was evaluated by placing 0.2 g DEX-loaded MBG microtubes into 250 mL SBF at 37 °C for 6, 24, 72, 120, 192, 360, 528 and 720 h.

2.4. Cell viability test

The MC3T3-E1 cells (ATCC) were routinely grown in an MEM medium (Gibco, Gaithersburg, MD, USA) supplemented with 10% fetal bovine serum (FBS; Sigma-Aldrich). The cells were plated on 96-well plates at an initial density of 1×10^5 per well in a humidified atmosphere with 5% CO_2 at 37 °C.

The viability of the MC3T3-E1 cells was determined using an MTT assay [25]. The cells treated with concentrations of MBG microtubes ranging from 0.1 to 10 μg mL^{-1} were harvested at 1, 3 and 7 days. A 100 μL aliquot of a 0.5 mg mL^{-1} MTT solution (Sigma-Aldrich, Australia) was added to each scaffold, and the cells were cultured for 4 h at 37 °C. Then, the upper medium was carefully removed, and the formazan was dissolved in 150 μL dimethyl sulfoxide (DMSO; Sigma-Aldrich). The absorbance was measured at 570 nm on a microplate reader (TECAN, Salzburg, Austria).

3. Characterization

Power X-ray diffraction (PXRD) measurements were obtained using a Siemens D5005 diffractometer. A Hitachi X-650B scanning electron microscope was used for SEM measurements. Transmission electron microscopy experiments were performed on a JEM1011 electron microscope with an acceleration voltage of 100 kV. The N_2 adsorption–desorption isotherms were recorded at 77 K using a Micromeritics ASAP 2010. The HPLC system consisted of an LC-10ADvp pump and an LC-2010A HT/2010C HT detector (SHIMADZU Co., Japan).

4. Results and discussion

4.1. Characterization of the MBG microtubes

MBG microtubes could be obtained through a sol–gel method using block copolymers of P123 and wool sponges as templates. The SEM images of the wool sponge and the as-prepared MBG microtubes were provided in Fig. 1(a)–(d) and revealed a highly ordered 1D tubular network. The MBG microtubes had a cylindrical structure, and most of tubes clearly exhibited hollow structures with many cava. The microtubes had a diameter of almost 10 μm and a length of approximately 50 μm–100 μm.

The powder XRD pattern of the synthesized MBG microtubes was shown in Fig. 2a. Only one diffraction peak could be observed in the small-angle regime ($2\theta = 1.06°$) and could be indexed to the (100) diffraction of a 2D hexagonal (p6 mm) lattice [15]. The disappearance of the (110) and (200) diffraction peaks was attributed to a perturbation of the interpenetrating macropores [26]. The XRD analysis was in agreement with

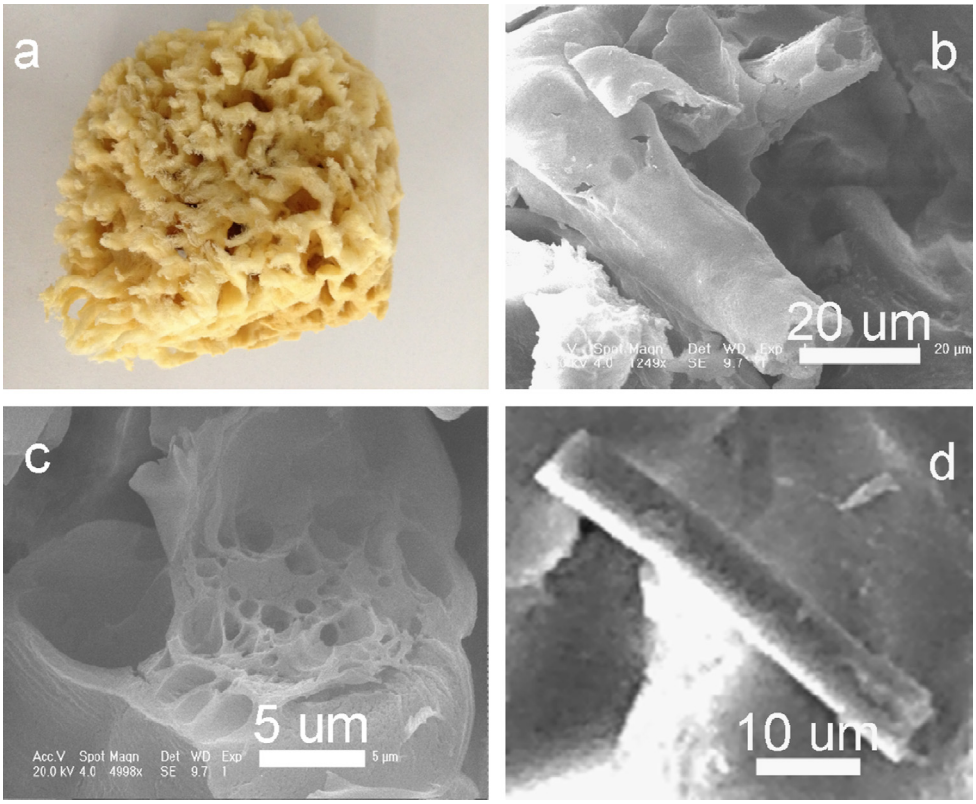

Fig. 1. (a) Photo of a wool sponge; (b)–(d) SEM images of calcined MBG microtubes.

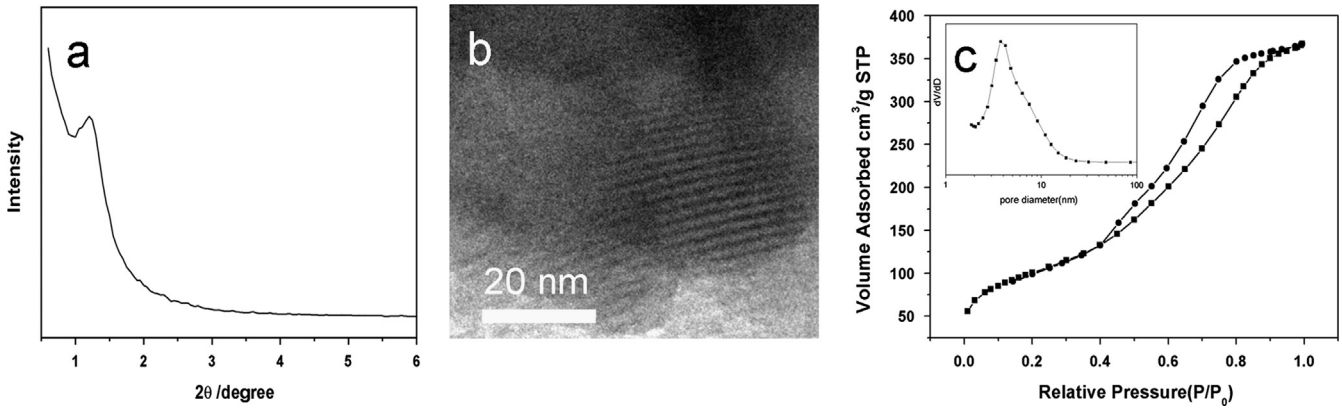

Fig. 2. (a) Small-angle powder XRD pattern of the synthesized MBG microtubes; (b) TEM image of the synthesized MBG microtubes; (c) the N_2 adsorption–desorption isotherms and the pore size of the synthesized MBG microtubes.

the TEM observations, as shown in Fig. 2b. Clearly, the typical characteristics of a hexagonally packed mesostructure were present.

The N_2 adsorption–desorption isotherms of the MBG microtubes were shown in Fig. 2c. The curves could be identified as type-IV isotherms, which were characteristic of mesoporous materials [15,27]. The samples exhibited type-H1 hysteresis loops in the mesopore range, which features the cylindrical pores. The narrow peak in the Barrett–Joyner–Halenda (BJH) pore-size distribution curve (inset) indicated uniformity in the mesopores in these materials.

In this experiment, the in vitro bone-forming activity of the MBG microtubes was tested in SBF to monitor the formation of hydroxycarbonate apatite (HCA) on the surface of the MBG microtubes. Fig. 3a provided the SEM micrograph of the MBG microtube surface after soaking in the SBF solution for 6 h. Prior to soaking in the SBF solution, the MBG microtubes exhibited a relatively smooth surface (Fig. 1(b)). The SEM image revealed that the surface of the MBG microtubes underwent important change when it reacted with the SBF. The surface was nearly covered with the newly formed plate-like HCA after soaking for 6 h [28], and the morphology had no obvious difference among the MBG microtubes as a function of time. Fig. 3b showed the wide-angle XRD patterns of the MBG microtubes before and after soaking in the SBF solutions at varying intervals. The two diffraction peaks

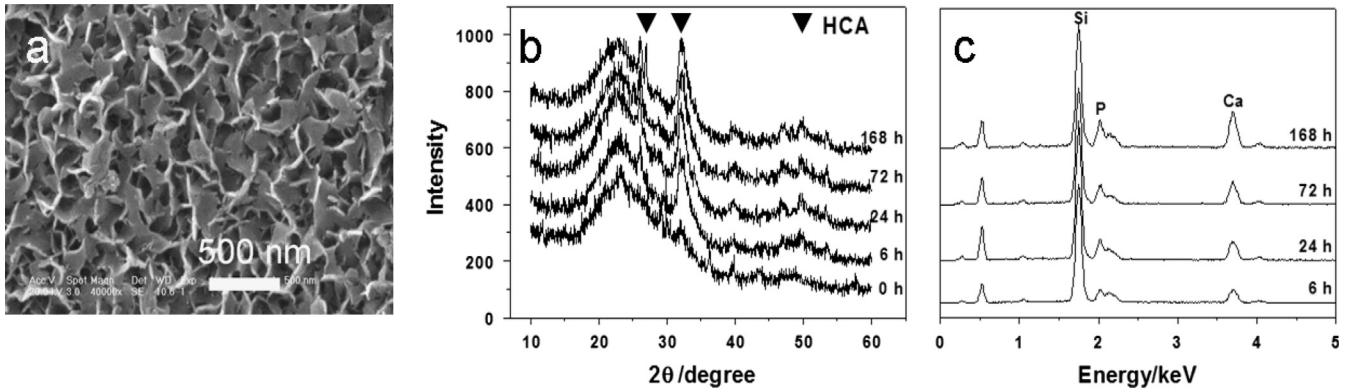

Fig. 3. (a) SEM image of the MBG microtubes before and after soaking in SBF for 6 h; (b) wide-angle XRD and (c) EDS patterns of the MBG microtubes before and after soaking in SBF for the following times.

characteristic of HCA at 26.02 and 32.18 corresponding to the (002) and (211) reflections could clearly be observed in the XRD pattern after soaking for 6 h. These peaks indicated the formation of HCA on the surface of the MBG microtubes [29,30]. After prolonged soaking, the intensities of the HCA peaks increase, which was indicative of an increase in the HCA content. The results obtained from XRD were also confirmed through an EDS analysis, as shown in Fig. 3c. After immersion in SBF, the Ca and P concentrations increased significantly, signifying the extended development of HCA [31].

In this study, DEX, a drug used to treat rheumatoid arthritis, was selected as the target. The HPLC results indicated that the MBG/DEX sample contained 45.6% DEX, which corresponded to 838.2 mg of DEX in a 1 g sample of the MBG microtubes. The adsorption of DEX from ethanol was studied by determining adsorption isotherms [32]. In Fig. 4, the corresponding isotherm was expressed as the amount DEX adsorbed per weight MBG microtubes, n/w, as a function of the equilibrium concentration of DEX in ethanol solution. It could be seen that the data for adsorptive uptake of DEX from ethanol by MBG microtubes showed Langmuir-type isotherms. The main interaction sites between the DEX and the MBG microtubes surface were thought to be hydrogen bonding; that was, formation of the hydrogen bonding between the OH groups of DEX with the OH groups on the surface.

Molecular desorption from the adsorbed phase and diffusion from within the pore structure of the matrices, referred to as drug release, had been interpreted via the same factors controlling the adsorption process, viz. pore structure, host-guest chemical interaction, and solvent chemical properties [33–35]. In the present study, the DEX release properties from MBG microtubes were investigated as a function of time as shown in Fig. 5. The mathematical theories were used to analyze the experimentally measured in vitro drug release kinetics and to determine the apparent diffusion coefficient of DEX within the MBG microtubes. The solution model was based on Fick's second law of diffusion [36,37]. Fig. 5 showed that the experimental release values did not deviate significantly from the mathematical model employed in this study (curves and symbols in Fig. 5). This indicated that drug release from these systems was primarily diffusion-controlled. Fig. 5

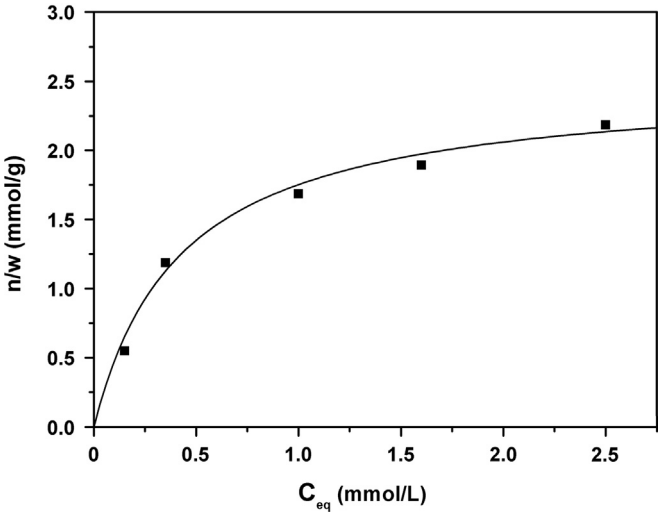

Fig. 4. The adsorption isotherm of DEX in ethanol solution for the MBG microtubes.

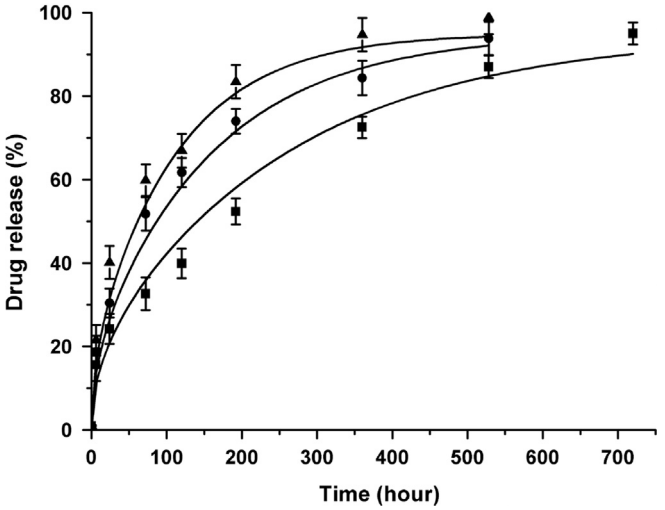

Fig. 5. Effects of initial drug content 1.0 mmol g^{-1}(▲), 1.6 mmol g^{-1} (●) and 2.5 mmol g^{-1} (■) on release of DEX from the MBG microtubes: theory (curves, Fick's second law of diffusion) and experiment (symbols). The data are presented as the mean value ± SD for three independent experiments.

showed the importance of the DEX amount (1.0, 1.6 and 2.5 mmol g^{-1}) on the release from the MBG microtubes. Based on these calculations, the diffusion coefficients of DEX within the MBG microtubes were 3.87×10^{-16} m^2/h, 6.27×10^{-16} m^2/h and 8.58×10^{-16} m^2/h, respectively. Clearly, the relative release rate decreased with increasing drug loading. The MBG microtubes also exhibited a considerably extended overall drug release of more than 30 days with increasing initial drug amount (2.5 mmol g^{-1}), confirming that this approach could achieve long and sustained drug release, which might be required, for example, for effective anti-infection bone therapy. Because a numerical approach based on Fick's second diffusion law was used to investigate drug release kinetics, the similar relationship was also observed by other researchers. Drug release profiles from porous hydroxyapatite tablets was studied by öner et al. and Vervaet et al. [32,37]. In their research, the slower drug release from the tablets was strictly related to the porous structure of the matrices (pore size, shape and connectivity). Pendleton et al. investigated drug delivery behavior of mesoporous silica SBA-15 containing the natural antibacterial allyl isothiocyanate (AITC) as model drugs [38]. The apparent drug diffusivity was depending on the mesoporous network. Analysis of the desorption or controlled release data, they gave effective diffusion coefficients of 4.40×10^{-16} m^2/s and 3.00×10^{-16} m^2/s for SBA-15 carriers. Effective diffusion coefficients were considerably higher than that in our system. The much slower rate of diffusion from within the MBG microtubes was, most probably, due to the porous structure of the matrices. The MBG microtubes had sustained drug delivery profiles due not only to the surface SiOH and the existing mesoporous phase but also to their 1D multichannel structures. This observation could be explained by two effects: (1) the multichannel microtubes could act as many micro-reservoirs providing a constant drug concentration differential inside and outside the microtubes [39] and (2) the 1D multichannel structures might play a key role in buffering the drug molecules, which increased the diffusion hindrance compared with the single mesoporous phase and maintained a constant diffusion.

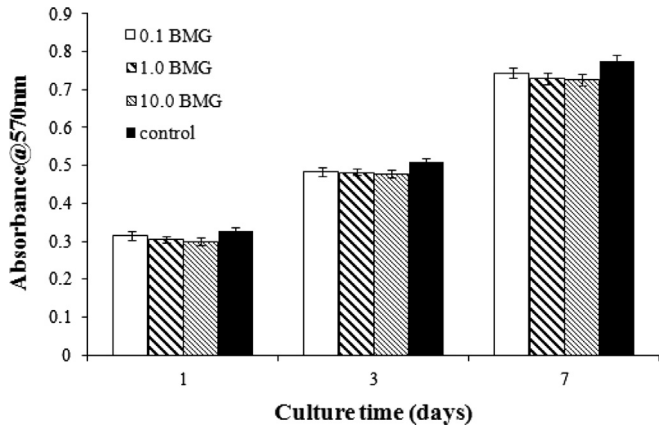

Fig. 6. The MTT assay of MC3T3-E1 cells cultured on concentrations of the MBG microtubes ranging from 0.1 to 10 μg ml^{-1} over different intervals. The data are presented as the mean value ± SD for three independent experiments.

As shown in Fig. 6, the MTT assay indicated that the concentrations of the MBG microtubes ranging from 0.1 to 10 μg mL^{-1} had no effect on the MC3T3-E1 cell viability. Moreover, no significant difference in the absorbance value was observed on the corresponding day. Consequently, good biocompatibility of the MBG microtubes depressed any toxicity reactions and the MBG microtubes had the potential for use in bio-applications.

5. Conclusion

In conclusion, 1D multichannel MBG microtubes with excellent in vitro bone-forming bioactivity could be prepared using the triblock copolymer P123 and wool sponges as structure-directing materials. The complex inner structures of the MBG microtubes could facilitate drug transport. Furthermore, the functional mesoporous bioactive glasses microtubes might find potential applications in tissue engineering and drug storage.

Acknowledgment

The work was supported by the National High Technology Research and Development Program (863 Program) (2011AA030102, 3R211L416604), the National Key Technology R&D Program (3G012Q386604) and the China Postdoctoral Science Foundation (801119606201, 801120036201).

References

[1] J.H. Jung, M.S. Park, S.J. Shinkai, Fabrication of silica nanotubes by using self-assembled gels and their applications in environmental and biological fields, Chemical Society Reviews 39 (2010) 4286–4302.
[2] C.C. Chen, Y.C. Liu, C.H. Wu, C.C. Yeh, M.T. Su, Y.C. Wu, Preparation of fluorescent silica nanotubes and their application in gene delivery, Advanced Materials 17 (2005) 404–407.
[3] Z.G. Feng, Y.S. Li, D.C. Niu, L. Li, W.R. Zhao, H.R. Chen, L. Li, M. L. Ruan, J.L. Shi, A facile route to hollow nanospheres of mesoporous silica with tunable size, Chemical Communications (2008) 2629–2631.
[4] L.L.J. Joongoo, J.C. Park, H.A. Song, Nanoreactor framework of a Au@SiO_2 yolk/shell structure for catalytic reduction of p-Nitrophenol, Advanced Materials 20 (2008) 1523–1528.
[5] Z.Y. Wang, D.Y. Luan, C.M. Li, F.B. Su, S. Madhavi, F.Y.C. Boey, X. W. Lou, Engineering nonspherical hollow structures with complex interiors by template-engaged redox etching, Journal of the American Chemical Society 132 (2010) 16271–16277.
[6] K. Kostarelos, A. Bianco, M. Prato, Promises, facts and challenges for carbon nanotubes in imaging and therapeutics, Nature Nanotechnology 4 (2009) 627–633.
[7] M. Prato, K. Kostarelos, A. Bianco, Functionalized carbon nanotubes in drug design and discovery, Accounts of Chemical Research 41 (2008) 60–68.
[8] R. Singh, J.W. Lillard, Nanoparticle-based targeted drug delivery, Experimental and Molecular Pathology 86 (2009) 215–223.
[9] P.A. Tran, L.J. Zhang, T.J. Webster, Carbon nanofibers and carbon nanotubes in regenerative medicine, Advanced Drug Delivery Reviews 61 (2009) 1097–1114.
[10] Z.F. Ji, G.F. Lin, Q.H. Lu, L.J. Meng, X.Z. Shen, L. Dong, C. Fu, X. Zhang, Targeted therapy of SMMC-7721 liver cancer in vitro and in vivo with carbon nanotubes based drug delivery system, Journal of Colloid and Interface Science 365 (1) (2012) 143–149.

[11] P.M. Rørvik, T. Grande, M.A. Einarsrud, One-dimensional nanostructures of ferroelectric perovskites, Advanced Materials 23 (2011) 4007–4034.
[12] G.R. Patzke, F. Krumeich, R. Nesper, Oxidic nanotubes and nanorods–anisotropic modules for a future nanotechnology, Angewandte Chemie International Edition 41 (14) (2002) 2446–2461.
[13] Y. Zhao, X.Y. Cao, L. Jiang, Bio-mimic multichannel microtubes by a facile method, Journal of the American Chemical Society 129 (2007) 764–765.
[14] Y. Zhao, L. Jiang, Hollow micro/nano materials with multilevel interior structures, Advanced Materials 21 (2009) 3621–3638.
[15] X.X. Yan, C.Z. Yu, X.F. Zhou, J.W. Tang, D.Y. Zhao, Highly ordered mesoporous bioactive glasses with superior in vitro bone-forming bioactivities, Angewandte Chemie International Edition 43 (44) (2004) 5980–5984.
[16] Q.H. Shi, J.F. Wang, J.P. Zhang, J. Fan, G.D. Stucky, Rapid-setting, mesoporous, bioactive glass cements that induce accelerated in vitro apatite formation, Advanced Materials 18 (2006) 1038–1042.
[17] C.T. Wu, Y. Ramaswamy, Y.F. Zhu, R.K. Zheng, R. Appleyard, A. Howard, H. Zreiqat, The effect of mesoporous bioactive glass on the physiochemical, biological and drug-release properties of poly(DL-lactide-co-glycolide) films, Biomaterials 30 (12) (2009) 2199–2208.
[18] H.M. Lin, W.K. Wang, P.A. Hsiung, S.G. Shyu, Light-sensitive intelligent drug delivery systems of coumarin-modified mesoporous bioactive glass, Acta Biomaterialia 6 (2010) 3256–3263.
[19] P.H. Yan, J.Q. Wang, J.F. Ou, Z.P. Li, Z.Q. Lei, S.R. Yang, Synthesis and characterization of three-dimensional ordered mesoporous–macroporous bioactive glass, Materials Letters 64 (2010) 2544–2547.
[20] J. Huang, T. Kunitake, Nano-precision replication of natural cellulosic substances by metal oxides, Journal of the American Chemical Society 125 (2003) 11834–11835.
[21] J. Huang, I. Ichinose, T. Kunitake, Nanocoating of natural cellulose fibers with conjugated polymer: hierarchical polypyrrole composite materials, Chemical Communications (2005) 1717–1719.
[22] Y.H. Zhang, X.Y. Liu, J.G. Huang, Hierarchical mesoporous silica nanotubes derived from natural cellulose substance, ACS Applied Materials and Interfaces 3 (9) (2011) 3272–3275.
[23] H.S. Wang, X.H. Gao, Y.N. Wang, J.L. Tang, C.C. Sun, X.L. Deng, X. D. Niu, Bio-templated synthesis of mesoporous bioactive glass with a hierarchical pore structure, Materials Letters 76 (2012) 237–239.
[24] T. Kokubo, H. Takadama, How useful is SBF in predicting in vivo bone bioactivity?, Biomaterials 27 (2006) 2907–2915
[25] M.C. Serrano, R. Pagani, M. Vallet-Regi, J. Pena, A. Ramila, I. Izquierdo, M.T. Portolés, In vitro biocompatibility assessment of poly(epsilon-caprolactone) films using L929 mouse fibroblasts, Biomaterials 25 (25) (2004) 5603–5611.
[26] O. Sel, D. Kuang, M. Thommes, B. Smarsly, Principles of hierarchical meso- and macropore architectures by liquid crystalline and polymer colloid templating, Langmuir 22 (5) (2006) 2311–2322.
[27] X.X. Yan, G.F. Wei, L.Z. Zhao, J. Yi, H.X. Deng, L.Z. Wang, G.Q. Lu, C.Z. Yu, Synthesis and in vitro bioactivity of ordered mesostructured bioactive glasses with adjustable pore sizes, Microporous and Mesoporous Materials 132 (2010) 282–289.
[28] H.S. Yun, S.E. Kim, E.K. Park, Bioactive glass–poly (ε-caprolactone) composite scaffolds with 3 dimensionally hierarchical pore networks, Materials Science and Engineering C 31 (2011) 198–205.
[29] Y. Minaberry, M. Jobbagy, Macroporous bioglass scaffolds prepared by coupling sol–gel with freeze drying, Chemistry of Materials 23 (2011) 2327–2332.
[30] X. Li, J.L. Shi, Y.F. Zhu, W.H. Shen, H. Li, J. Liang, J.H. Gao, A template route to the preparation of mesoporous amorphous calcium silicate with high in vitro bone-forming bioactivity, Journal of Biomedical Materials Research Part B Applied Biomaterials 83B (2) (2007) 431–439.
[31] C.T. Wu, Y.H. Zhou, W. Fan, P.P. Han, J. Chang, J. Yuen, M. Zhang, Y. Xiao, Hypoxia-mimicking mesoporous bioactive glass scaffolds with controllable cobalt ion release for bone tissue engineering, Biomaterials 33 (7) (2012) 2076–2085.
[32] M. öner, E. Yetiz, E. Ay, U. Uysal, Ibuprofen release from porous hydroxyapatite tablets, Ceramics International 37 (2011) 2117–2125.
[33] J. Andersson, J. Rosenholm, S. Areva, M. Linden, Influences of material characteristics on ibuprofen drug loading and release profiles from ordered micro- and mesoporous silica matrices, Chemistry of Materials 16 (21) (2004) 4160–4167.
[34] C. Charnay, S. Begu, C. Tourne-Peteilh, L. Nicole, D.A. Lerner, J.M. Devoisselle, Inclusion of ibuprofen in mesoporous templated silica: drug loading and release property, European Journal of Pharmaceutics and Biopharmaceutics 57 (2004) 533–540.
[35] G. Cavallaro, P. Pierro, F.S. Palumbo, F. Testa, L. Pasqua, R. Aiello, Drug delivery devices based on mesoporous silicate, Drug Delivery 11 (2004) 41–46.
[36] J. Crank, The Mathematics of Diffusion, 2nd ed., Oxford University Press, Oxford, 1975.
[37] A. Cosijns, C. Vervaet, J. Luyten, S. Mullen, F. Siepman, L. Van Hoorebek, B. Masschaele, V. Cnuddan, J.P. Remon, Porous hydroxyapatite tablets as carriers for low-dosed drugs, European Journal of Pharmaceutics and Biopharmaceutics 67 (2) (2007) 498–550.
[38] S.Y. Park, P. Pendleton, Mesoporous silica SBA-15 for natural antimicrobial delivery, Powder Technology 223 (2011) 77–82.
[39] K. Gulati, S. Ramakrishnan, M.S. Aw, G.J. Atkins, D.M. Findlay, D. Losic, Biocompatible polymer coating of titania nanotube arrays for improved drug elution and osteoblast adhesion, Acta Biomaterialia 8 (2012) 449–456.